Numeric simulation of relativistic stellar core collapse and the formation of Reissner-Nordström black holes

Cristian R. Ghezzi* and Patricio S. Letelier†

Department of Applied Mathematics, Instituto de Matemática, Estatística e Computação Científica, Universidade Estadual de Campinas, Campinas, São Paulo, Brazil

(Received 1 September 2004; revised manuscript received 8 November 2006; published 12 January 2007)

The time evolution of a set of $22M_{\odot}$ unstable charged stars that collapse is computed integrating the Einstein-Maxwell equations. The model simulates the collapse of a spherical star that had exhausted its nuclear fuel and has or acquires a net electric charge in its core while collapsing. When the charge-to-mass ratio is $Q/\sqrt{G}M \geq 1$, the star does not collapse but spreads. On the other hand, a different physical behavior is observed with a charge-to-mass ratio of $1 > Q/\sqrt{G}M > 0.1$. In this case, the collapsing matter forms a bubble enclosing a lower density core. We discuss an immediate astrophysical consequence of these results that is a more efficient neutrino trapping during the stellar collapse and an alternative mechanism for powerful supernova explosions. The outer space-time of the star is the Reissner-Nordström solution that matches smoothly with our interior numerical solution; thus the collapsing models form Reissner-Nordström black holes.

DOI: 10.1103/PhysRevD.75.024020 PACS numbers: 04.70.Bw, 04.25.Dm, 04.40.Nr

I. INTRODUCTION

In this work we intend to study the effects of an electric field on the collapse of a massive star. We perform direct relativistic simulations assuming spherical symmetry and integrating the Einstein-Maxwell equations. We study the collapse of several stars with different values of the total electric charge and determine the limits at which the collapse is avoided by the effect of the repulsive electric field. The electric charge is carried by the particles that compose the collapsing fluid. The electromagnetic field and the internal energy of the gas contribute to the total mass-energy of the star, so it is not clear whether it is possible to overcharge a collapsing configuration. The analysis and conclusions drawn for collapsing charged shells cannot be directly extrapolated for this case, and a complete relativistic calculation performed in a self-consistent way is needed to know the outcome of the charged collapse.

In particular, we found the formation of a bubble that was not predicted before. Although its theoretical explanation is quite natural, the formation of the bubble depends on the initial conditions, and its evolution is far from obvious due to the nonlinearities of the Einstein-Maxwell equations. Numerical solutions for the problem of charged stellar collapse were found only recently [1,2].

It is commonly assumed that the stars are nearly neutrally charged due to a mechanism of selective accretion of charges from the surrounding interstellar medium. Therefore, if a star is initially positively (negatively) charged, accretion of negative (positive) charges from the surrounding gas will tend to neutralize the total net charge. The same reasoning is applied to black holes [3,4]. We observe that, to our knowledge, the effects of selective accretion were never fully calculated. On the other hand, a star can be electrically neutral while possessing a huge internal electric field [5].

The internal electric field of an astronomical object can be very large in some special scenarios [6–9]. In particular, the charge separation inside a spherical compact star, in hydrostatic equilibrium, can be very large when one of the plasma components is a degenerate gas while the other is a Maxwell-Boltzmann gas, like the gas of degenerated electrons and the gas of nuclei in a white dwarf [7].

The calculations presented in this paper correspond to the case in which the star possesses a net electric charge. However, the results can be taken as an approximation to the more complicated problem of a star with a total charge of zero and with a nonzero internal electric field. We leave this point aside and, for clarity, we will concentrate here on the dynamics of a star with a total positive charge.

We ask whether an electrically charged star can collapse to form a charged black hole. Would the Coulomb repulsion avoid the collapse of the star, and, moreover, are there physical differences with the physics of uncharged collapse? Furthermore, from pure analytic analysis it is not clear if it is possible to form an overcharged black hole (with $Q > \sqrt{G}M$). The dynamics of a collapsing star could be quite different from the collapse of a charged shell onto an already formed Reissner-Nordström (RN) black hole, mainly due to backreaction effects. In the present paper, we will try to give the answers to these questions.

Extremely charged black holes ($Q/\sqrt{G}M = 1$) represent an extreme limit in the context of the cosmic censorship hypothesis, since bodies with charge equal to or higher than the extremal value are undressed by event horizons and constitute naked singularities [3,10]. On the other hand, the formation of RN black holes is in connection with the third law of black hole thermodynamics [1,11,12],

*Electronic address: ghezzi@ime.unicamp.br
†Electronic address: letelier@ime.unicamp.br

because an extreme RN black hole has zero temperature. So, there is an interest in the formation of charged black holes from a pure theoretical point of view [13].

In this paper we are not concerned with the mechanisms that produce a charge or an internal electric field. Neither magnetic fields nor rotations are taken into account, although they could increase the magnitude of the electric fields.

Without loss of generality, the density of the charge was chosen proportional to the density of rest mass. The interior solutions found can be matched smoothly with the Reissner-Nordström exact solution for the vacuum spacetime [1]. Therefore, in the cases in which the star collapses, the result is the formation of a Reissner-Nordström black hole.

The paper is organized as follows. In Sec. II, we discuss the problem of charged collapse, analyzing the order of magnitude of the physical quantities. In Sec. III, the general relativistic equations that govern the dynamics of the stellar core collapse are described. In Sec. IV, the numerical techniques used to integrate the general relativistic equations and some caveats on their applications are described. Section V brings a discussion and interpretation of the numerical results. In Sec. VA, we derive the formula for the maximum mass for Newtonian charged cold compact stars, and in Sec. V B we calculate the optical depth for the neutrinos emitted during the collapse and the implications for core collapse supernova. We also discuss the implications for core collapse supernova. We end in Sec. VI by presenting some final remarks.

II. SOME ORDER OF MAGNITUDE ESTIMATES

In this section we show some order of magnitude estimates, in order to put in a clear perspective the problem of a self-gravitating charged fluid sphere. The calculations in the present section are valid only in the nonrelativistic regime.

The formation of a charged star is possible when the gravitational attraction overwhelms the electrostatic repulsion on each single particle of the gas that is collapsing, i.e.,

$$F_{\text{grav}} \geq F_{\text{elect}}, \tag{1}$$

or equivalently

$$qQ_s \geq mM_s, \tag{2}$$

where Q_s and M_s are the charge and mass of the star and q and m are the charge and mass of the particles. In this section we use a Newtonian approach; the full relativistic case could be different.

Assume a star that has a total charge-to-mass ratio $Q_s/\sqrt{G}M_s$. According to Eq. (2) any particle with a charge-to-mass ratio $q/\sqrt{G}m$ can be added to the star if

$$\alpha_1 \equiv \frac{Q_s}{\sqrt{G}M_s} \leq \left(\frac{q}{\sqrt{G}m}\right)^{-1}, \tag{3}$$

where the equality gives the maximal charge-to-mass ratio

$$\alpha_1 = \left(\frac{q}{\sqrt{G}m}\right)^{-1}. \tag{4}$$

For example, a proton has a charge-to-mass ratio $q_p/\sqrt{G}m_p \sim 10^{18}$. Using Eq. (3) the proton can be added to the charged star if

$$\frac{Q_s}{\sqrt{G}M_s} \leq 10^{-18}. \tag{5}$$

Thus, a star with higher charge-to-mass ratio cannot be assembled from protons alone. On the other hand, if the infalling particles are dust particles with a larger charge-to-mass ratio, the maximum limit for the charge-to-mass ratio of the charged star can be much higher.

An example of this is a self-gravitating ball of an Fe nucleus, of mass M_{ball} and charge Q_{ball}. As the charge-to-mass ratio for Fe is $q/\sqrt{G}m \sim 10^{16}$, Eq. (3) for Fe gives

$$\alpha_2 = \frac{Q_{\text{ball}}}{\sqrt{G}M_{\text{ball}}} \leq 10^{-16}, \tag{6}$$

and we see that in this case $\alpha_2 \gg \alpha_1$ [greater than for protons alone; see Eq. (5) above].

For "charged dust" formed by particles with $q/\sqrt{G}m \sim 1$, a self-gravitating sphere with mass M_{dust} and charge Q_{dust} can be in hydrostatic equilibrium if

$$\alpha_3 = \frac{Q_{\text{dust}}}{\sqrt{G}M_{\text{dust}}} \sim 1. \tag{7}$$

So, $\alpha_3 \gg \alpha_2 \gg \alpha_1$. Let us estimate the amount of charge needed to have an extremely charged $10M_\odot$ star. In this case $Q_{\text{star}}/\sqrt{G}M_{\text{star}} = 1$, so

$$\begin{aligned} Q_{\text{star}} &= \sqrt{6.6710^{-8}} \times 10 \times 1.910^{33} \\ &= 4.9 \times 10^{30} \text{ statcoulomb}. \end{aligned} \tag{8}$$

Therefore, we need to have an excess of

$$\sim Q_{\text{star}}/q_p = 10^{40} \text{ charges}$$

in the star, where $q_p = 4.803 \times 10^{-10}$ statcoulomb is the charge of one proton. There are roughly $\sim 10^{58}$ baryons in a $10M_\odot$ star. So, there must be one charged particle on $\sim 10^{18}$ neutral ones in order to have a maximally charged compact object. This is compatible with the limits given above. Therefore, in the extremal case, there is a small charge imbalance equal to

$$\delta Q \sim 10^{-18} \text{ charges per baryon} \tag{9}$$

in the star—a tiny amount of charge from a microscopic point of view, but with a huge total sum (see Ref. [1]).

It is possible to make the objection that the nucleus would disintegrate, or suffer nuclear fission, before assembling a charged star. However, the energy locally available (in the center of mass of the particles) from the collapse is not enough to unbind a nucleus (bounded by the strong force). This was calculated for a compact charged neutron star. An exception is a nearly extremal compact object, which, in this case, is energetically favorable for the nucleus to disintegrate [1]. The conclusion is that we can approach the formation of a "nearly extreme" object, although it is not possible to reach the extremal value, as the particles will fission first (see [1] for details).

Studying theories with extra dimensions, Mosquera Cuesta and coworkers [14] found that particles located in the brane can leak out to the bulk space. The result is that electrons can leak out more easily than baryons, producing a charge asymmetry that can be very large in very old stellar systems. This is suitable for type II supernova progenitors and neutron stars [1]. The mechanism produces a charge imbalance of [14]

$$\delta Q \sim 10^{-14}\text{–}10^{-16} \text{ charges per baryon.} \tag{10}$$

This is several orders of magnitude higher than the needs for producing an extremal star. Therefore, charged old stars must be considered and studied as a theoretical possibility.

III. EQUATIONS IN COMOVING COORDINATES

We want to solve the Einstein-Maxwell equations (see Ref. [1]):

$$R^{\mu\nu} - \frac{1}{2} g^{\mu\nu} R = \frac{8\pi G}{c^4} T^{\mu\nu}, \tag{11}$$

where $R^{\mu\nu}$ is the Ricci tensor, $g^{\mu\nu}$ is the metric tensor, R is the scalar curvature, and $T^{\mu\nu}$ is the energy-momentum tensor, composed of two parts:

$$T^{\mu\nu} = T_F^{\mu\nu} + T_M^{\mu\nu}, \tag{12}$$

where $T_F^{\mu\nu}$ is the perfect fluid energy-momentum tensor and $T_M^{\mu\nu}$ is the Maxwell energy-momentum tensor. The electromagnetic energy-momentum tensor is given by

$$T_M^{\mu\nu} = \frac{1}{4\pi}\left(F^{\mu\alpha}F^{\nu}{}_{\alpha} - \frac{1}{4} g^{\mu\nu} F_{\alpha\beta}F^{\alpha\beta}\right). \tag{13}$$

Here $F^{\mu\nu}$ is the Maxwell electromagnetic tensor, which can be written in terms of a potential A^{μ}:

$$F_{\mu\nu} = A_{\mu;\nu} - A_{\nu;\mu}. \tag{14}$$

In the last equation and in the rest of the paper, we use a semicolon to denote the covariant derivative. The perfect fluid energy-momentum tensor is

$$T_F^{\mu\nu} = (P + \delta c^2) u^{\mu} u^{\nu} - P g^{\mu\nu}, \tag{15}$$

where δc^2 is the density of mass-energy and P is the pressure, given in [dyn/cm^2], and u^{ν} is the 4-velocity of the observers comoving with the fluid [1,15,16]. The electromagnetic tensor must satisfy the Maxwell equations [1,17,18]:

$$F^{\mu\nu}{}_{;\nu} = 4\pi j^{\mu}. \tag{16}$$

From Eq. (14) and using the Bianchi identities, we have

$$F_{[\alpha\beta;\gamma]} = 0. \tag{17}$$

We will use the common split of the energy:

$$\delta = \rho(1 + \epsilon/c^2), \tag{18}$$

where ρ is the rest mass density, and $\rho\epsilon$ is the internal energy density [1,19].

The fluid must satisfy the energy-momentum conservation equation

$$T^{\mu\nu}{}_{;\nu} = 0, \tag{19}$$

and the baryon conservation equation

$$(\rho u^{\nu})_{;\nu} = 0. \tag{20}$$

We will write the Einstein-Maxwell equations in coordinates and gauge choice appropriated for its numeric implementation [1]. Considering a spherical star, the line element in comoving coordinates is given by

$$ds^2 = a(t, \mu)^2 c^2 dt^2 - b(t, \mu)^2 d\mu^2 - R(t, \mu)^2 d\Omega^2. \tag{21}$$

The 4-velocity of an observer comoving with the fluid is $u^{\nu} = [a^{-1}, 0, 0, 0]$, and satisfies $u^{\nu} u_{\nu} = c^2$, where c is the speed of light. The coordinate μ was gauged to be the rest mass enclosed by comoving observers standing on spherical layers of the star. Each layer has its own constant value of μ. In particular, observers at the surface of the star will be designated with a coordinate $\mu = \mu_s$.

We define [20]

$$u = R_{,t}/a.$$

So, the equation of motion, obtained from the Einstein-Maxwell equations [1], is

$$u_{,t} = -a\left[4\pi R^2 \frac{\Gamma}{w}\left(P_{,\mu} - \frac{QQ_{,\mu}}{4\pi R^4}\right) + \frac{Gm}{R^2} + \frac{4\pi G}{c^2} PR - \frac{GQ^2}{c^2 R^3}\right], \tag{22}$$

where $w = 1 + \epsilon/c^2 + P/\rho c^2$ is the relativistic specific enthalpy, ρ is the rest mass density, ϵ is the internal energy per unit mass, P is the pressure, G is the gravitational constant, $Q(\mu)$ is the total charge integrated from the origin of coordinates up to the spherical layer with coordinate μ, and $m = m(t, \mu)$ is the total mass-energy defined below. We use the notation $f_{,x} = \partial f/\partial x$, with $x = \{\mu, t\}$, throughout the paper.

We note that Eq. (22) resembles a Newtonian equation of motion plus relativistic corrections. In Eq. (22) the last two terms are pure relativistic, and the full equation is equivalent to its Newtonian counterpart when $c \to \infty$

[21]. The factor Γ is a generalization of the special-relativistic γ factor for general relativity and is given by

$$\Gamma^2 = 1 + \frac{u^2}{c^2} - \frac{2mG}{Rc^2} + \frac{GQ^2}{c^4R^2}. \tag{23}$$

This factor also verifies the equality $\Gamma = R_{,\mu}/b$ (see Refs. [1,17,22]).

The equation for the metric component $a = g_{tt}^{1/2}/c$ is obtained from the energy-momentum conservation equation $T^{\nu}_{1;\nu} = 0$, and is given by [1]

$$\frac{(aw)_{,\mu}}{aw} = \frac{1}{wc^2}\left[\epsilon_{,\mu} + P\left(\frac{1}{\rho}\right)_{,\mu} + \frac{QQ_{,\mu}}{4\pi R^4\rho}\right]. \tag{24}$$

The other independent component $T^{\nu}_{0;\nu} = 0$ gives

$$\epsilon_{,t} = -P\left(\frac{1}{\rho}\right)_{,t}, \tag{25}$$

which is identical to the nonrelativistic adiabatic energy conservation equation, and constitutes the first law of thermodynamics. We observe that Eq. (25) does not contain any electromagnetic term. This is due to the symmetry of the problem, although an electromagnetic term arises in the total energy [see Eq. (28) below].

From the conservation of the number of baryons, we obtain the equation for the metric component $b = g_{\mu\mu}^{1/2}$ [1],

$$b(t, \mu) = \frac{1}{4\pi R^2\rho}. \tag{26}$$

The Lagrangian coordinate μ can be chosen to be [1]

$$\mu = 4\pi \int_0^{R'} \rho R^2 dR/\Gamma. \tag{27}$$

This is the total rest mass enclosed by a sphere of circumference $2\pi R'$. Thus, the collapsing ball is divided in layers of constant rest mass μ, and each comoving observer is at rest in each of these layers [23].

The equations for the total mass and the mass conservation are, respectively [1],

$$m(t, \mu) = 4\pi \int_0^{\mu} \rho\left(1 + \frac{\epsilon}{c^2}\right)R^2 R_{,\mu} d\mu + \frac{1}{c^2}\int_0^{\mu} \frac{QQ_{,\mu}}{R} d\mu, \tag{28}$$

$$(\rho R^2)_{,t}/\rho R^2 = -a u_{,\mu}/R_{,\mu}. \tag{29}$$

The charge 4-current j^{ν} is the product of a scalar electric charge density $\rho_{\rm ch}$ times u^{ν}; $j^{\nu} = \rho_{\rm ch} u^{\nu}$. It can be shown that the charge and the rest mass are conserved in shells comoving with the fluid [1,17]. So, the charge increment between layers can be written as being proportional to $d\mu$,

$$dQ = 4\pi\rho_{\rm ch} R^2 dR/\Gamma, \tag{30}$$

where $\rho_{\rm ch} \propto \rho$.

We observe that Eq. (30) is a nonlinear equation, since Γ depends on the integral value of the charge $Q(\mu)$ [see Eq. (23)]. Therefore, the set of equations above must be solved self-consistently.

Equations (22)–(30) are solved numerically with the following boundary conditions:

$$P = 0, \quad \text{at} \quad \mu = \mu_s, \quad \forall\ t, \tag{31a}$$

$$a = 1, \quad \text{at} \quad \mu = \mu_s, \quad \forall\ t, \tag{31b}$$

$$u = 0, \quad \text{at} \quad t = t_0, \quad \forall\ \mu, \tag{31c}$$

$$R = 0, \quad \text{at} \quad \mu = 0, \quad \forall\ t, \tag{31d}$$

where μ_s is the mass coordinate at the surface of the star. The boundary condition (31a) can be derived from the matching condition between the interior and the exterior solution [1]. Equation (31b) expresses our coordinate freedom to choose the time synchronized with a comoving observer moving with the surface of the star. Equation (31c) means that the ball is initially at rest (at the initial time t_0), and Eq. (31d) is the impenetrability condition at the origin of coordinates (this condition can be stated equivalently as $u = 0$ at $\mu = 0$). In the next section we will present the initial conditions.

In this work we choose

$$\rho_{ch} = \text{constant} \times \rho, \tag{32}$$

for simplicity and without loss of generality.

IV. NUMERICAL TECHNIQUES AND CODE SETUP

The equations given in the section above are written in a form closely paralleling the equations of May and White [1,24], for the noncharged case [22,25–28].

We built the numerical code collapse05v2 to integrate Eqs. (22)–(30).

Equation (24) is rewritten as [1]

$$aw = a_0 w_0 \exp\left[\int_0^{\mu_s}\left(d\epsilon + Pd\left(\frac{1}{\rho}\right) + \frac{QdQ}{4\pi r^4\rho}\right)/wc^2\right]. \tag{33}$$

This equation is integrated numerically from the surface of the star toward the center, using the boundary condition $a_s w_s = 1$, where a_s and w_s are given at the surface of the star (with the coordinate μ_s); note that we already chose $a_s = 1$ [see Eq. (31b)].

The collapse05v2 uses a leapfrog method plus a predictor corrector step, and iterates with a Crank-Nicholson algorithm. The method is second order accurate in time and space. We use a numerical viscosity to resolve the strong shock waves formed [25].

A. Initial conditions and numerical caveats

We assume a charge density proportional to the rest mass density through the star: $\rho_{\rm ch}/\sqrt{G}\rho \sim$ constant.

From Eqs. (27) and (30) we see that $Q(\mu)/\sqrt{G}\mu =$ constant, $\forall(t, \mu)$.

We assume a polytropic equation of state, $P = k\rho^{\gamma}$, where $\gamma = 5/3$ is the adiabatic coefficient [29]. The star initially has a uniform mass density, $\rho = 10^7$ g cm^{-3}, and a uniform distribution of electric charge density, in all the models studied. The initial specific internal energy ϵ is varied in the different simulations. The initial setup imitates a massive star of $M = 21.035M_{\odot}$ that had exhausted its nuclear fuel. Its fate depends on the internal energy and charge of the initial configuration. This is explored with our simulations. The initial radius of the star is $R_0 = 10^9$ cm, in all the simulations.

Also, we consider that the electric field is always much lower than the Schwinger field limit for pair creation ($\sim 10^{16}$ Volt/cm, in *vacuo* and in flat space-time [30]). For example, in the case of extremal charge $Q/\sqrt{G}M = 1$, the total charge will be $Q \sim 10^{31}$ statcoulomb. In this case, the maximum electric field strength is $\sim 10^{11}$ stat-Volt/cm or $\sim 3 \times 10^{15}$ Volt/cm. However, during the collapse the field can strengthen and take higher values, so quantum effects would be taken into account in a more realistic approach. We are not considering magnetic fields in the present simulations [31].

The simulations converge toward the same solution when the resolution or the viscosity parameter is changed. The parameters of the simulation were chosen for accuracy and efficiency when running on a single processor. We performed the simulations using an Intel Pentium IV 2.6 Ghz processor (32 bits) and compiled the code with LAHEY/FUJITSU V6.1 [32] for 32 bits; also, we used an AMD Athlon FX 2.6 Ghz processor (64 bits) and compiled with ABSOFT [33] for 64 bits, running under a Linux operating system. The code also runs under the Windows operating system and compiles with the Fortran 90 Power Station. We did not find essential differences between the different runs with the exception of the speed of the simulation, which is faster with the AMD processor. In addition we set (a) the number of integration points to 1000, (b) the viscosity parameter to 3.3, and (c) the initial time-step to 10^{-5} sec. We also performed test simulations with 300 and 1500 points to be sure of the physical results, and tested the code, varying the viscosity over a wide range of parameters. In the present simulations we tried to minimize the effects of the viscosity while keeping the ability of the code to resolve shock fronts.

The percentage of numerical error in the Hamiltonian constraint, expressed by the conservation of the total mass-energy $m(t, \mu_s)$, is given by

$$E_H = 100 \times |m - m'|/m,$$

where $m' = m'(\mu_s)$ is the exact value of the total mass-energy (constant in time) and $m = m(t, \mu_s)$ is the numerical value. The momentum constraint is "built in" the code and exactly conserved. In the present simulations, $E_H <$ 0.1% when the AH forms, using 1000 points, and it is $E_H < 0.009\%$ with 1500 points, with no essential qualitative differences between the solutions. These values of E_H are for the worst case of a large binding energy and with very strong shocks, so they can be considered as the superior bounds of the error.

After crossing the AH, the error grows to $\sim$0.4% (using 1000 points), and the simulation is stopped. Thus, in every simulation we set a maximum error tolerance of $E_H \sim 0.4\%$. We checked that, by using a higher number of points, the errors are reduced.

We emphasize that the numerical errors (mainly E_H, not the roundoff errors) and the intrinsic difficulty on the simulation are in the formation of the black hole region, because near it several numerical operators blow up.

B. The apparent horizon

For each layer of matter with the Lagrangian coordinate μ, it is possible to define an internal and an external horizon,

$$r_{\pm}(t, \mu) = \frac{Gm(t, \mu)}{c^2} \pm \frac{G}{c^2}\sqrt{m^2(t, \mu) - Q^2(\mu)/G}, \quad (34)$$

which can be interpreted as a generalization of the Schwarzschild radius for charged stars. During the simulation, an apparent horizon (AH) forms when some layers of matter cross its external horizon, i.e. when $r(t, \mu) \leq r_{+}(t, \mu)$ [1]. In addition to the formation of the apparent horizon, in some cases a coordinate singularity develops, i.e. $g_{tt}(t, \mu') \to 0$ and $g_{\mu\mu}(t, \mu') \to +\infty$ (for some coordinate value $\mu' \neq 0$). Note that at the coordinate $\mu = 0$ the physical timelike singularity of the vacuum Reissner-Nordström space-time is located. The simulation must end before any observer μ can meet its internal horizon $r_{-}(\mu)$. Hence, we cannot say if the star collapses directly to a singularity or if it passes through a wormhole to another asymptotically flat universe. In this paper, we leave this question open.

The formation of an AH is a sufficient condition (although not necessary) for the formation of an event horizon and a black hole region [1]. Moreover, the interior solution matches with the exterior Reissner-Nordström space-time [1]. In this sense, we can say that the outcome of the simulations in which an AH forms is the formation of a "Reissner-Nordström black hole." Of course, if not all the matter collapses to the AH, the result at the moment the simulation is stopped will be an electric black hole plus a surrounding gas with a vacuum Reissner-Nordström exterior space-time.

We observe that there must exist other formulations of the problem in which it is possible to get closer to the singularity while avoiding the AH. We will explore this subject in future works.

TABLE I. Simulations of the collapse of a massive star varying the charge-to-mass ratio and the binding energy.

Simulation	Charge-to-mass ratio $Q/\sqrt{Gm}$	ϵ[a] (ergs/c^2)	Binding energy[b]	Collapse?	Shell?
1	0.484	9.61×10^{-7}	-2.994×10^{-2}	yes	yes
2	0.484	1.92×10^{-6}	-2.992×10^{-2}	yes	no
3	0.484	2.88×10^{-6}	-2.990×10^{-2}	yes	no
4	0.484	1.44×10^{-3}	$+2.498 \times 10^{-4}$	no	no
5	0.484	1.35×10^{-3}	-1.764×10^{-3}	no	no
6	0.145	1.15×10^{-6}	-3.830×10^{-2}	yes	no
7	0.145	9.61×10^{-8}	-3.833×10^{-2}	yes	no
8	0.145	9.61×10^{-9}	-3.833×10^{-2}	yes	yes
9	0.290	9.61×10^{-7}	-3.583×10^{-2}	yes	no
10	0.290	9.61×10^{-8}	-3.584×10^{-2}	yes	yes
11	0.290	9.61×10^{-10}	-3.585×10^{-2}	yes	yes
12	0.850	9.61×10^{-7}	-1.073×10^{-2}	yes	yes
13	0	9.61×10^{-7}	-3.740×10^{-2}	yes	no
14	≥ 1.0	...	...	no	no

[a]The energy density is initially distributed uniformly on the star in all the simulations. The equation of state is $P = k\rho^\gamma$ with $\gamma = 5/3$. The mass of the star in every simulation is $M = 21.035 M_\odot$.
[b]The binding energy of the star, $(m - \mu)c^2$, in units of $\mathbf{M}_\odot c^2$ ergs.

V. DISCUSSIONS OF THE RESULTS

We performed a set of simulations on the collapse of a $21M_\odot$ star, varying the initial conditions. We found that for certain cases a shell-like structure of higher mass density and charge is formed in the most external part of the star. This shell enlarges with time until it reaches the center of the star.

Table I summarizes the results of the simulations performed. In each model studied are different amounts of total electric charge and initial internal energy (or binding energy). The fate of each model depends on these conditions.

The formation of the shell is sensible to the internal energy, or the binding energy, of the star (see Table I). The stronger the bound of the star, the higher the wall of the shell.

In Fig. 1, we show the profiles of the mass density versus the Lagrangian mass μ for model 3 of Table I; in this case, the shell forms only mildly. However, there is a strong shock wave formed. Figure 2 shows the velocity profiles, on which a strong shock propagating outwards is seen. We observe that, although the shock is propagating outwards, the sign of the fluid velocity is negative everywhere, indicating that the star is always collapsing. There is an

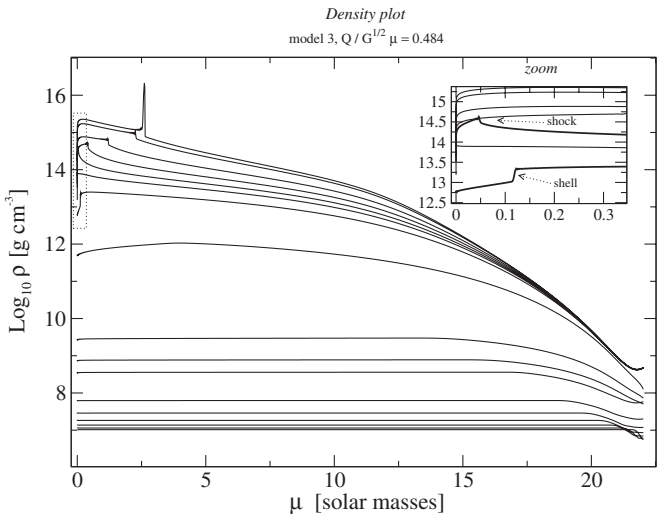

FIG. 1. Snapshots of the mass density versus the mass coordinate μ, for model 3 of Table I. The shell forms mildly in this case, although the shock is very strong.

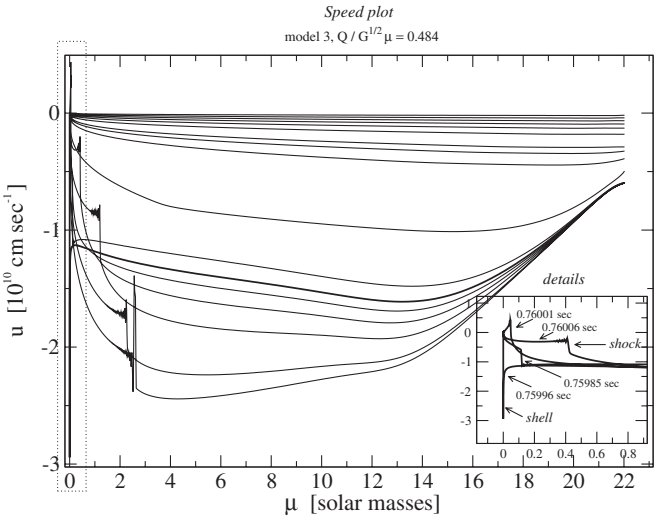

FIG. 2. Snapshots of the speed versus the Lagrangian mass. The inset shows the details of the shell impinging on the center and the shock starting its propagation. The speed is positive during a short lapse of time.

exception in which the shock velocity acquires a positive sign, although it lasts a very brief period of time. This is shown on the inset of Fig. 2: the shell is reaching the coordinate center. After that, a shock wave is formed and starts to propagate outwards. During a brief lapse of time, the velocity is positive, although the shock is not strong enough to stop the total collapse. Figure 3 contains the snapshots of the metric component $g_{tt}^{1/2}$: it can be seen that, concordant with the shell impinging the center, g_{tt} acquires a value greater than 1, indicating a blueshift with respect to the infalling matter. The inset of Fig. 3 shows the details of the jumps produced on the value of $g_{tt}^{1/2}$ at the shell and at the shock positions, as well as the mentioned blueshift.

Figure 4 contains the snapshots of the mass density for model 11 of Table I. In this case there is a strong shell formed. In this figure we can see that the shell propagates inwards, to lower values of the Lagrangian coordinate μ, until it impinges the center. At this moment, and place, a strong shock is formed that starts its outward propagation. The inset box of Fig. 4 is a zoom of the dotted box, showing the details of the collapsing shell and the shock formed. Figure 5 shows the verification that the collapse produces a black hole. In spherical symmetry the apparent horizon is formed simply when an observer crosses his/her own Schwarzschild radius. The inset box of Fig. 5 shows the radius profile at the moment that the curve touches the Schwarzschild radius profile at a point. That point indicates an observer crossing the Schwarzschild radius and is the *locus* of the apparent horizon. After that, the apparent horizon will evolve, approaching the event horizon at infinite coordinate time or after complete collapse (not calculated).

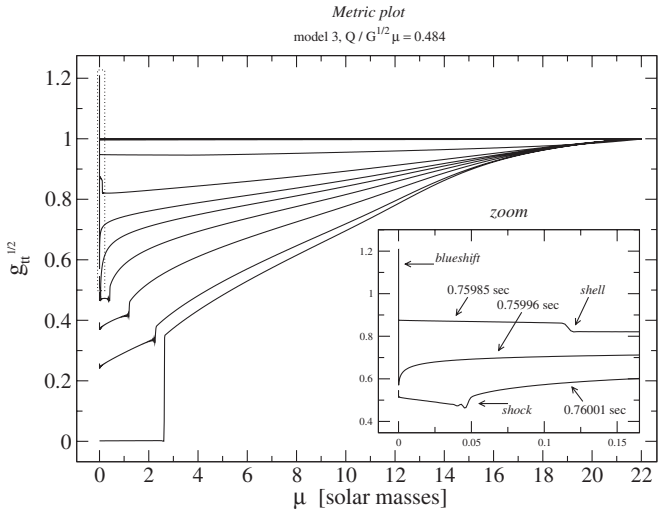

FIG. 3. Snapshots of the coefficient $g_{tt}^{1/2}$. A sharp discontinuity is distinguished at the shock and shell positions. The inset shows a zoom of the dotted box; the coefficient $g_{tt}^{1/2}$ is greater than 1 at the instant of time the shock forms the sign of the velocity, indicating a blueshift with respect to the infalling matter. The shock and the shell are indicated in this figure.

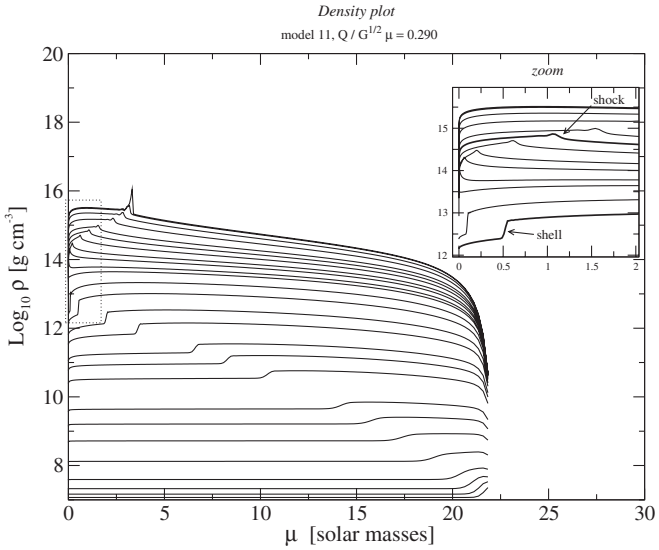

FIG. 4. Snapshots of the mass density versus μ, for model 11 of Table I. In this case there is an important imploding shell. The dotted box is zoomed on the inset, which shows the shell impinging at the center and the shock forming and propagating outwards.

Figure 6 shows the velocity profiles for model 11; there is a strong shell and a strong shock in this case. However, the velocity has a negative sign and the matter collapses directly to a black hole. Figure 7 shows the speed profile at the moment of time in which the shell impinges the center, and the formation and propagation of the shock wave. The inset box shows a close-up of the details. There is a short

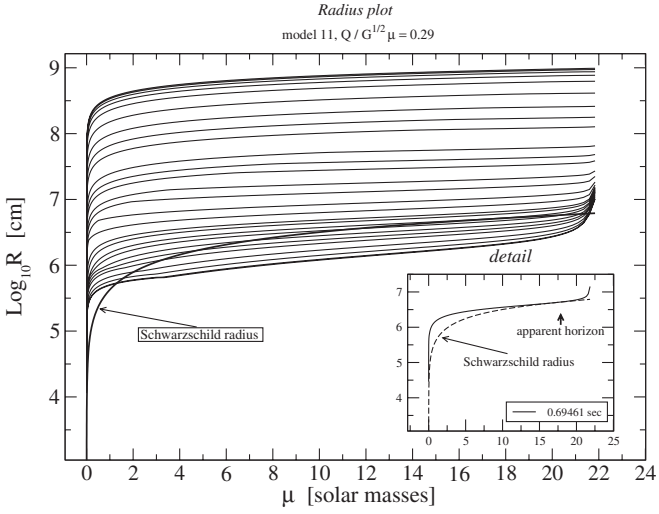

FIG. 5. The radius ($\log_{10}$Radius) versus the Lagrangian mass. The bold line shows the Schwarzschild radius at the instant of the apparent horizon formation; the inset box shows the detail of an observer crossing his/her own Schwarzschild radius (an arrow is pointing to the observer) and signaling the formation of an apparent horizon. It can be appreciated that the simulation continues far beyond the formation of the apparent horizon.

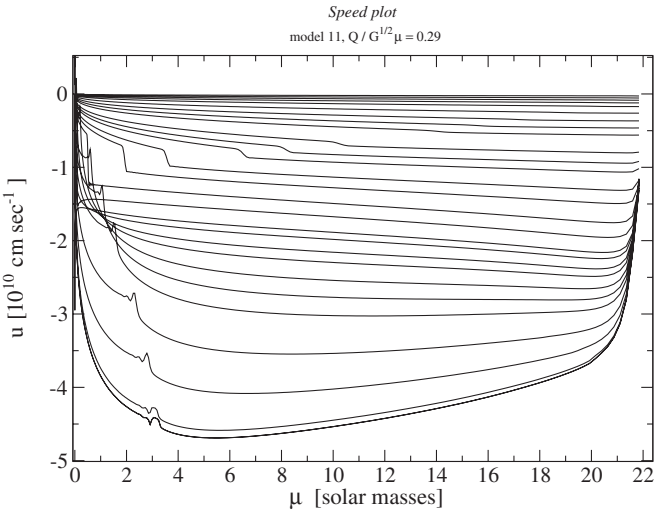

FIG. 6. Snapshots of the speed versus μ for model 11. A jump in the velocity profile can be observed at the shell position, dislocating through the center of the star. See Fig. 7.

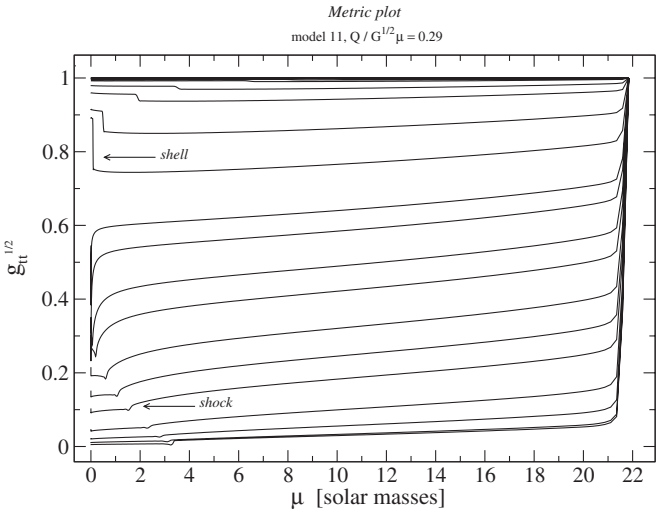

FIG. 8. Temporal snapshots for $\sqrt{g_{tt}}$ versus μ for model 11 and its late collapse to zero. We must observe that the apparent horizon forms before $g_{tt} \to 0$, which indicates the convergence towards the event horizon.

lapse of time in which the shock has positive velocity. Figure 8 shows the metric coefficient $g_{tt}^{1/2}$ going to zero. In this case g_{tt} never becomes greater than 1, and the inner matter is always redshifted with respect to observers standing at the surface of the star or outside it.

Figure 9 shows the density snapshots for the collapse of an uncharged star (model 13). It is possible to compare this simulation with the former simulations; we see that for the charged collapse the density profiles are flatter all the way through the black hole formation. Figure 10 shows the velocity profiles (compare with Figs. 2 and 6). Figure 11 shows the collapse of $g_{tt}^{1/2}$ (compare with the Figs. 3 and 8).

Figure 12 shows the profiles of the metric function R; the bold line is the Schwarzschild radius at the moment the apparent horizon forms. The inset box shows the detail of the radius profile touching the Schwarzschild profile at one point, signaling the formation of an apparent horizon at the point indicated with the vertical arrow, at the time indicated on the legend box. The simulation is continued beyond that event, as seen in this figure.

It is possible to compare the profile of the mass-energy function for the charged collapse with very strong shocks (model 3, Fig. 13) with the case of uncharged collapse (model 13, Fig. 14). The inset box of Fig. 13 shows a zoom of the right end of the curves which indicates the level of energy conservation in the simulation. All curves must

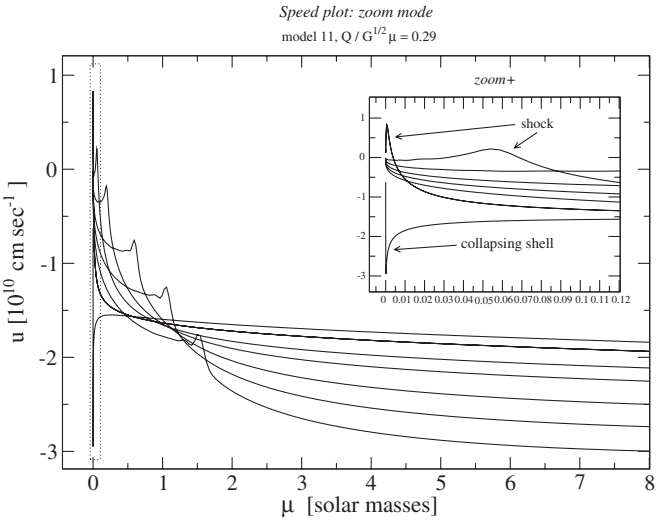

FIG. 7. Detail of the speed's profile, showing the moment of time the shell impinges at the center of the star. Later, the shock is formed and starts its outward propagation; the inset shows a zoom of the dotted box. See Fig. 6.

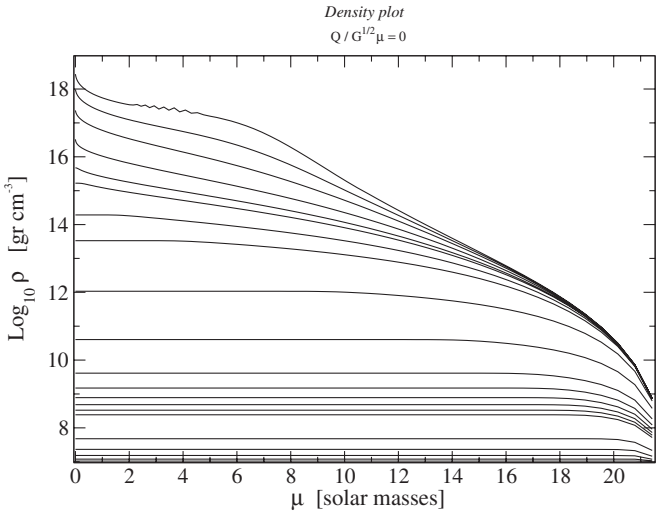

FIG. 9. Snapshots of the mass density versus μ for model 13, an uncharged star.

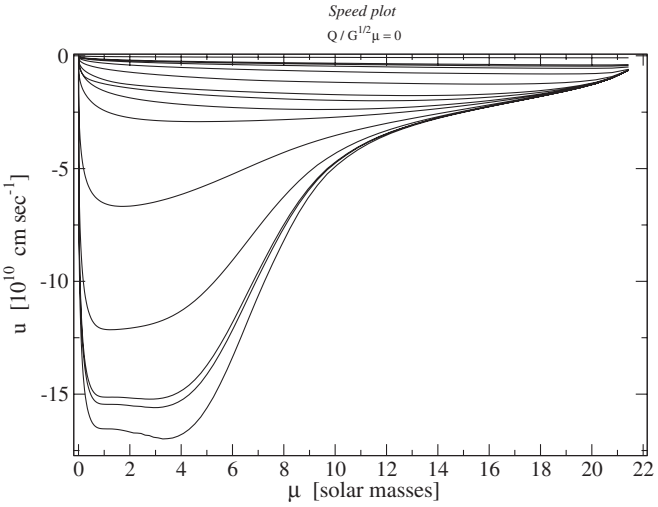

FIG. 10. Snapshots of the speed profile, where u is the rate of radius change per unit proper (comoving) time change.

reach the same point for perfect energy conservation. At the moment of the apparent horizon formation, the mass-energy is conserved with a precision of 99.98%, which is an excellent value taking into account that this is the worst case. After the apparent horizon formation, the good conserving property is lost as in any relativistic code, and the simulation ends with a 0.48% error. We emphasize that this is the physical quantity we use to check the convergence properties of our code, since the momentum constraint is conserved exactly by the algorithm. As was said before the simulations were performed using 1000 points, and the conservation can be better using a larger number of points. Figure 14 represents the energy conservation for the case of uncharged collapse. The precision is roughly the same as in the former case, although using only 100 points. We checked that by using 1000 points the errors are lowered by a factor of 10 in this case, i.e., 99.998% precision at the apparent horizon formation. The reason for better conser-

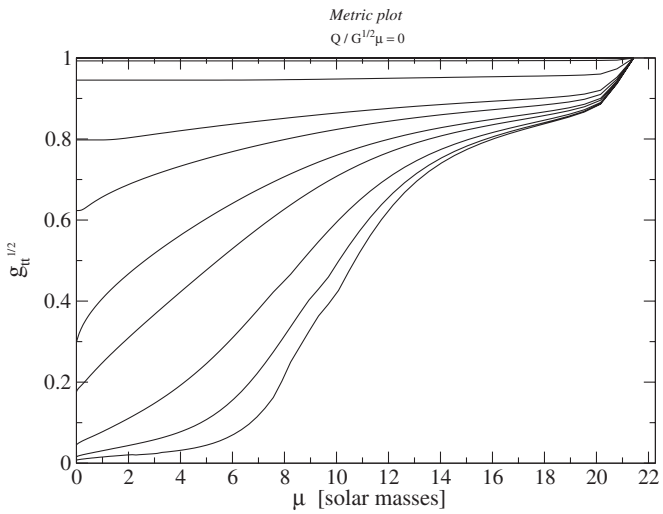

FIG. 11. Temporal snapshots for $\sqrt{g_{tt}}$ versus μ for model 13.

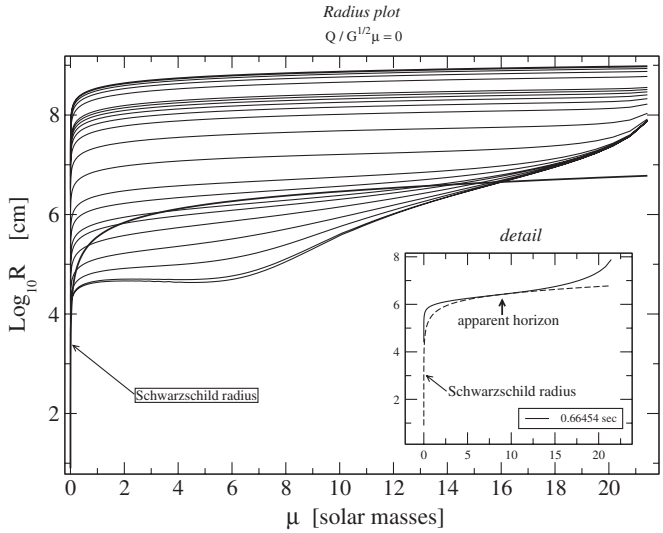

FIG. 12. The radius versus μ. The bold line shows the Schwarzschild radius at the instant of time the apparent horizon is formed; the inset shows the detail of an observer (an arrow is pointing to the observer) crossing his/her own Schwarzschild radius, indicating the formation of an apparent horizon at this coordinate and at the time indicated.

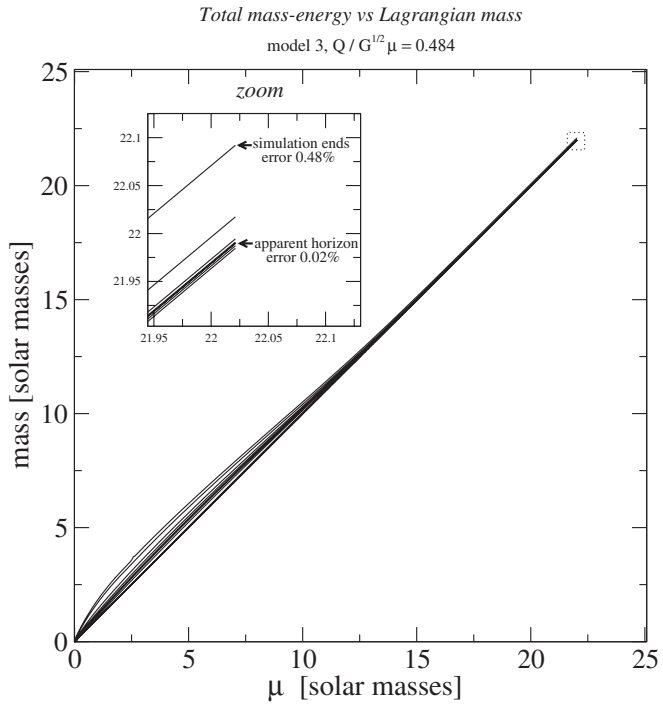

FIG. 13. Snapshots for the mass-energy versus μ for model 3. The numerical error in the simulation of the models can be measured by the failure of the curves to converge at the same point; this is indicated in the zoom box. After the apparent horizon formation, the error is 0.02% for model 3 and model 13. The same error is found for model 13 using a lower number of radial points (see text for details). Compare with Fig. 14.

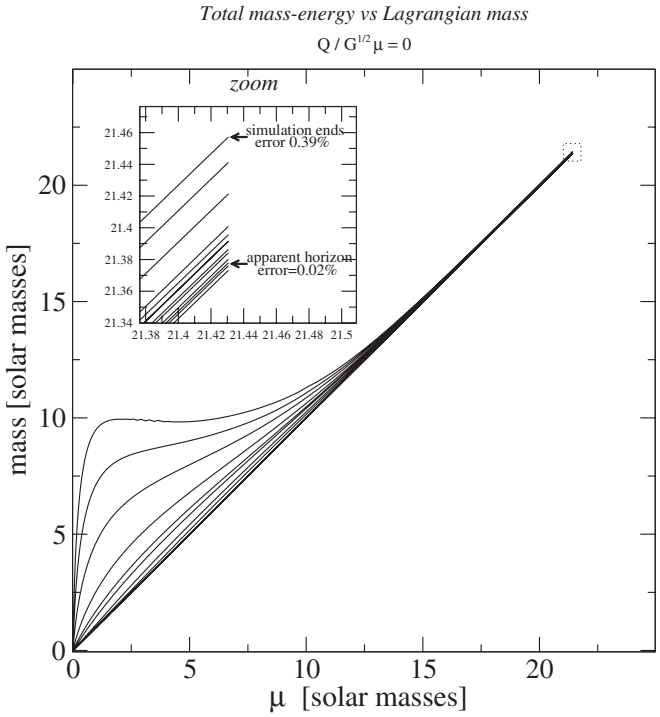

FIG. 14. Snapshots for the mass-energy versus μ for model 13. The numerical error in the simulation of the models can be measured by the failure of the curves to converge at the same point; this is indicated in the zoom box. After the apparent horizon formation, the error is 0.02% for model 3 and model 13. The same error is found for model 13 using a lower number of radial points (see text for details). Compare with Fig. 13.

vation of the energy constraint is that there are not very strong shocks like in the former simulations.

The explanation of the shell formation can be grasped from the equation of motion [Eq. (22)]. This effect can also happen in Newtonian physics, but its evolution in the strong field regime is highly nonlinear and far from obvious. It seems difficult to make a complete analytic description of its evolution. However, starting with a ball of constant rest mass density and charge, it is easy to see that a shell must be formed. The relativistic term GQ^2/c^2R^3, in Eq. (22), produces a repulsion of the matter on the initial homogeneous sphere, which in turn produces a charge gradient $QQ_{,\mu}/4\pi R^4$.

The term $QQ_{,\mu}/4\pi R^4$ in the equation of motion can be important in supporting the weight of the star [see Eq. (22)]. Near the surface of the star, the pressure gradient term $P_{,\mu}$ cancels the charge gradient term $QQ_{,\mu}/4\pi R^4$ at a certain point we call μ_0. Since at this point the two terms cancel out, all the matter outside the layer of coordinate μ_0 is almost in free fall, producing an accumulation of matter and giving rise to the shell, while at coordinates with $\mu < \mu_0$ the matter is supported by a positive net gradient. We carefully checked that this is not a numerical artifact, changing the boundary conditions at the surface, the amount of charge, and the initial conditions.

Hence, the result is that the point μ_0 is roughly the *locus in quo* the term $P_{,\mu}(\mu_0)$ and the term $QQ_{,\mu}/4\pi R^4(\mu_0)$ sum zero; then the gas is compressed and a shell of matter forms.

The nonlinearity in the strong field regime comes from the fact that Γ is a function of the charge and the mass, and multiplies the two gradient terms, enhancing the effect [see Eq. (22)].

From all the numerical experiments we performed, we observed that the shell formation effect arises more clearly when the initial density profile is flat. For the case of charged neutron star collapse, the effect is negligible [1].

The point μ_0 shifts to lower values with time, and this causes the shell to enlarge until $\mu_0 = 0$, when it reaches the origin and rebounds forming the shock wave mentioned above. It is observed that the shock does not form in the uncharged case, using the same set of initial conditions. The density contrast between the shell and its interior is higher for greater total charge (or, equivalently, a higher internal electric field and zero total charge). This is because the Coulomb repulsion inside the shell will be higher, and this gives a higher compression of the matter at the shell. The Coulomb repulsion term together with the pure relativistic term aGQ^2/c^2R^3 in Eq. (22) are responsible for the positive mass density gradient near the coordinate origin. The charged collapse is slightly delayed with respect to the uncharged one, i.e., ~ 0.75 sec for model 1 with respect to the uncharged case that lasts ~ 0.66 sec. At the end of the simulation, we observe that the density profile looks globally flatter and the maximum density value is lower than in the uncharged case.

Case 14 in Table I is special because it represents stars with a charge greater than or equal to the extremal value. We verified that in these cases the star expands "forever," i.e., we follow its expansion until the density gives a machine underflow. In any of these cases we expect a recollapse of the matter: the binding energy per nucleon tends to zero when the charge tends to the mass (see [1]), and is negative for a charge greater than the mass.

A. The maximum mass limit

For charged stars, there must exist a maximum mass limit like for uncharged compact stars. For white dwarfs, the limit is known as the Chandrasekhar mass limit, while for neutron stars it is the Oppenheimer-Volkoff limit, etc. In this section, we calculate the mass limit for Newtonian charged compact stars. We assume, for simplicity, an equation of state dominated by electrons [34],

$$P/\rho = Y_e kT/m_B + K_\gamma Y_e^\gamma \rho^{\gamma-1}. \tag{35}$$

For a spherical configuration, the Newtonian hydrostatic equilibrium gives

$$P_c/\rho_c = GM/R - Q^2/(4\pi R^4 \rho). \tag{36}$$

Simplifying the two equations, for $T = 0$ and $\gamma = 4/3$ we

get $(GM^2 - Q^2)/M^{4/3} = KY_e^{4/3}$. From these equations, we obtain the limiting mass $M_{\max}$. Assuming the charge is a fraction α of the mass, i.e., $Q = \alpha\sqrt{G}M$,

$$M_{\max} = \left(\frac{K}{G(1-\alpha^2)}\right)^{3/2} Y_e^2 \sim 5.83 \frac{Y_e^2}{(1-\alpha^2)} M_\odot, \quad (37)$$

which reduces to the known Chandrasekhar mass formula when $\alpha = 0$ (no charge), modulo some geometric factor depending on the density profile.

For the extreme case $\alpha = 1$, the configuration disperses to infinity. We checked that this also happens in the relativistic case (see model 14 of Table I).

B. Implications for core collapse supernovae

The quantity of energy deposition behind the formed shock wave is critical to produce a successful supernova explosion, like in the proposed mechanisms for core collapse supernovae explosions [35–37]. In the cases we studied, the shock wave is not fast enough to reach the surface of the star before the apparent horizon forms ahead of it, and the shock ends trapped by the black hole region. However, when including neutrino transport in our simulations, the shell formation could have a dramatic effect.

This provides a new mechanism for a successful core collapse supernova explosion. Although the calculations performed in the present work are far from complete supernova calculations, it is simple to show that in the charged collapse there is a more efficient energy deposition to revive the supernova shock wave.

As the density profile is flatter than in the uncharged case, the neutrino-sphere and gain radius for neutrino deposition must be different. In order to show this, we consider the change in the radius R_ν, of the neutrino sphere, which is defined by $\tau(R_\nu) = 2/3$, where the optical depth of the uncharged matter for the neutrinos is [35]

$$\tau(R) = 1.5 \times 10^{11}(N^2/6A)\epsilon_\nu^2 R^{-2}. \quad (38)$$

According to the numerical results presented, we make the approximation $\rho \sim$ constant, for the charged case, in order to obtain an analytic expression for the optical depth for neutrinos. In this case, the optical depth of the charged matter is

$$\tau_{\rm ch}(R) = 10^{-8}(N^2/6A)\epsilon_\nu^2 \rho_{12}(R_s - R). \quad (39)$$

It can be seen that $\tau_{\rm ch} \gg \tau$. Assuming typical values [35], $\epsilon_\nu = 10$ Mev and $\rho \sim 2 \times 10^{10}$ g cm^{-3}, in the uncharged case the position of the neutrino sphere is at $R_\nu \sim 110$ km, and in the charged case [38] it is $R_\nu \sim 845$ km. This implies a more efficient neutrino trapping during the charged collapse, and hence a more efficient energy deposition.

VI. FINAL REMARKS

We have performed relativistic numeric simulations for the collapse of spherical symmetric stars with a polytropic equation of state and possessing a uniform distribution of electric charge. We have not studied in this paper how the matter acquires a high internal electric field before or during the collapse process.

In the present model we studied the essential features of the collapse of stars with a total electric charge. The simulations are an approximation to the more realistic problem of the temporal evolution of a star with a strong internal electric field and total charge zero. This model is under consideration by the authors.

In the cases where the stars formed an apparent horizon, the formation of a Reissner-Nordström black hole is unavoidable. This is guaranteed by the singularity theorems and by the Birkhoff theorem.

For low values of the charge-to-mass ratio $Q/\sqrt{G}M \ll 1$, no difference with the collapse of an uncharged star was found. The value of the total charge that prevents the collapse of the star with any initial condition is given by a charge-to-mass ratio $Q/\sqrt{G}M \geq 1$. This means that stars with $Q/\sqrt{G}M \geq 1$ spread and do not collapse to form black holes or stars in hydrostatic equilibrium. A dramatically different physical behavior is observed when $Q/\sqrt{G}M > 0.1$. In this case, the collapsing matter forms a shell-like structure, or bubble, surrounding an interior region of lower density and charge. The effect is due to the competence between the Coulomb electrostatic repulsion and the attraction of gravity. This effect must occur in nonrelativistic physics as well. The relativistic case is more interesting due to the nonlinearity of the Einstein equations. The effect is more important when the internal energy of the star is lower (see Table I). In some of the experiments we observe a blueshift produced at the bouncing shock wave (see Fig. 3), because the strong shock wave acquires a positive velocity over a small lapse of time.

For all the cases studied, the density profile is globally flatter than in the uncharged collapse.

The optical depth for neutrinos is much higher in the case of the charged collapse; hence, the neutrino trapping must be more efficient. In conclusion, if the internal electric field increases during the stellar collapse, the formation of the shell must be taken seriously in supernova simulations.

In addition, we obtained the mass limit formula for Newtonian charged stars, which clearly precludes the formation of naked singularities. The mass limit cannot be naively extrapolated for the relativistic case, because charge and pressure regeneration effects can change the maximum charge-to-mass ratio. However, in the present work, we checked that it is not possible to form a star from matter with a charge-to-mass ratio greater than or equal to 1, in agreement with our mass formula and with the cosmic censorship conjecture.

A more complete simulation, including neutrino transport and other quantum effects, is being considered by the authors.

ACKNOWLEDGMENTS

The authors acknowledge the Brazilian agency FAPESP. This work benefited from useful discussions with Dr. Samuel R. Oliveira and Dr. Eduardo Gueron. We acknowledge Gian Machado de Castro for a critical reading of the manuscript. The simulations were performed at the Parallel Computer Lab., Department of Applied Mathematics, UNICAMP (Campinas State University).

[1] C. R. Ghezzi, Phys. Rev. D **72**, 104017 (2005); gr-qc/0510106.
[2] In the literature there are numerical and analytical solutions of charged spherical stars in hydrostatic equilibrium (see, for example, Refs. [12,39,40]). There is also numerical research on the collapse of charged scalar fields, with particular emphasis on the mass inflation effect near the Cauchy horizon [41] (and references therein), and global analysis on the mass inflation effect on the stellar collapse [42]. The physics of charged thin shell collapse has been analyzed in [11,43,44]. The equations for charged collapse were obtained in Refs. [17,18], and were rederived and integrated numerically in [1].
[3] R. Wald, *General Relativity* (University of Chicago Press, Chicago, 1984).
[4] N. K. Glendenning, *Compact Stars* (Springer-Verlag, New York, 2000).
[5] The total charge of a star can be zero, while its internal electric field is huge. Examples of this are charge separation effects in compact stars (see Refs. [6,7]); charge separation during accretion of matter onto a star or onto a black hole (see Refs. [45,8]); electric field generation due to magneto-rotational effects [46]; electric fields in pulsars [47]; and net charge effects due to physics in extra dimensions [14]. See also Refs. [4,48–51]
[6] E. Olson and M. Bailyn, Phys. Rev. D **12**, 3030 (1975).
[7] E. Olson and M. Bailyn, Phys. Rev. D **13**, 2204 (1976).
[8] V. F. Shvartsman, Sov. Phys. JETP **33**, 475 (1971).
[9] Ya. B. Zeldovich and I. D. Novikov, *Stars and Relativity*, edited by K. S. Thorne and W. D. Arnett (Dover Publications, Mineola, New York, 1971), Vol. 1, p. 451.
[10] P. S. Joshi, *Global Aspects in Gravitation and Cosmology* (Oxford Science Publications, New York, 1996).
[11] W. Israel, Phys. Rev. Lett. **57**, 397 (1986).
[12] P. Anninos and T. Rothman, Phys. Rev. D **65**, 024003 (2001); W. Israel, Phys. Rev. Lett. **57**, 397 (1986).
[13] Electromagnetic fields play an important role in several models for the inner engine of gamma ray bursts. During the accretion of plasma onto a black hole, the electromagnetic field can annihilate above a certain limit due to quantum effects, and produce a ''dyadosphere'' of electron-positron pairs that in turn annihilate to produce a gamma ray burst [50].
[14] Herman J. Mosquera Cuesta, A. Penna-Firme, and A. Perez-Lorenzana, Phys. Rev. D **67**, 087702 (2003).
[15] L. D. Landau and E. Lifshitz, *The Classical Theory of Fields* (Addison-Wesley, Reading, Massachusetts, 1961).
[16] S. Weinberg, *Gravitation and Cosmology: Principles and Applications of the General Theory of Relativity* (John Wiley & Sons, New York, 1972).
[17] J. D. Bekenstein, Phys. Rev. D **4**, 2185 (1971).
[18] B. Mashhoon and M. H. Partovi, Phys. Rev. D **20**, 2455 (1979).
[19] S. L. Shapiro and S. A. Teukolsky, *Black Holes, White Dwarfs, and Neutron Stars* (John Wiley & Sons, New York, 1983).
[20] This is the u^1 component of the comoving observer's 4-velocity in Schwarzschild coordinates; see Ref. [1] for details.
[21] In the hydrostatic limit we can take $u_{,t} = 0$ in Eq. (22) to obtain the Tolman-Oppenheimer-Volkov equation for charged stars [1].
[22] M. M. May and R. H. White, Phys. Rev. **141**, 1232 (1966).
[23] The definition of the Lagrangian mass coordinate is independent of the presence of electromagnetic fields [1].
[24] C. R. Ghezzi and P. S. Letelier, in *The Tenth Marcel Grossmann Meeting: On Recent Developments in Theoretical and Experimental General Relativity, Gravitation and Relativistic Field Theories*, edited by Mário Novello, Santiago Pérez Bergliaffa, and Remo Ruffini (World Scientific, Singapore, 2006); C. R. Ghezzi and P. S. Letelier, gr-qc/0312090.
[25] M. M. May and R. H. White, Methods Comput. Phys. **7**, 219 (1967).
[26] C. W. Misner and D. H. Sharp, Phys. Rev. **136**, B571 (1964).
[27] J. R. Oppenheimer and H. Snyder, Phys. Rev. **56**, 455 (1939).
[28] A. I. Voropinov, V. L. Zaguskin, and M. A. Podurets, Soviet Astronomy **11**, 442 (1967).
[29] For $\gamma =$ constant shocks see [52], p. 128.
[30] J. Schwinger, Phys. Rev. **82**, 664 (1951).
[31] A warning must be given: a magnetic field is induced in the collapsing charged sphere if perturbed slightly, and the spherical symmetry of the problem is broken. However, the strength of the induced magnetic field can be neglected in a first approximation to the full problem, as long as $|v|^2/c^2 \ll 1$, with v the nonradial component of the 3-velocity of the fluid. In the present case, $v = 0$.
[32] Lahey Computer System Inc., www.lahey.com.
[33] Absoft Fortran compiler, www.absoft.com.
[34] See Ref. [19] for the uncharged case.
[35] H. A. Bethe, Astrophys. J. **412**, 192 (1993).

[36] S. A. Colgate and R. H. White, Astrophys. J. **143**, 626 (1966).
[37] J. R. Wilson, in *Numerical Astrophysics*, edited by J. M. Centrella, J. M. LeBlanc, and R. L. Bowers (Jones & Bartlett, Boston, 1985), p. 422.
[38] From the simulations, we obtain the radius $R_s = 954$ km, at which $\rho = 2 \times 10^{10}$ g cm^{-3}, for the particular case $Q/\sqrt{GM} = 0.48$.
[39] F. de Felice, S. M. Liu, and Y. Q. Yu, Classical Quantum Gravity **16**, 2669 (1999).
[40] S. Ray, A. L. Espindola, M. Malheiro, J. P. S. Lemos, and V. T. Zanchin, Phys. Rev. D **68**, 084004 (2003).
[41] Y. Oren and T. Piran, Phys. Rev. D **68**, 044013 (2003).
[42] E. Poisson and W. Israel, Phys. Rev. Lett. **63**, 1663 (1989).
[43] D. G. Boulware, Phys. Rev. D **8**, 2363 (1973).
[44] J. E. Chase, Nuovo Cimento B **67(2)**, 136 (1970).
[45] J. A. de Diego, D. Dultzin-Hacyan, J. G. Trejo, and D. Núñez, astro-ph/0405237.
[46] B. Punsly, Astrophys. J. **498**, 640 (1998).
[47] P. Goldreich and W. H. Julian, Astrophys. J. **157**, 869 (1969).
[48] J. Bally and E. R. Harrison, Astrophys. J. **220**, 743 (1978).
[49] S. Rosseland, Mon. Not. R. Astron. Soc. **84**, 720 (1924).
[50] R. Ruffini, J. D. Salmonson, J. R. Wilson, and S.-S. Xue, Astron. Astrophys. **359**, 855 (2000); **350**, 334 (1999).
[51] S. Vauclair and G. Vauclair, Annu. Rev. Astron. Astrophys. **20**, 37 (1982).
[52] A. J. Chorin and J. E. Marsden, *The Mathematical Introduction to Fluid Mechanics* (Springer-Verlag, New York, 1990), 2nd ed.